An Effective Mechanical Design and Realization of a Humanoid Robot BUrobot

Davut Akdas

Electrical and Electronics Engineering Department, MMF, Balikesir University
Cagis, 10145, Balikesir, Turkey
akdas@balikesir.edu.tr

Abstract: Mechanical design and production of humanoid robots are not yet standardized and many different robot configurations are being researched by academics. This paper is written as a motivation to publish the results of an experimental study that was carried out at Balikesir University. The research project was aimed to explore whether a simpler, yet functional mechanical design aspects of humanoid robots with a relatively small budget could be achieved. Design process includes iterative mechanical design including motor selection, kinematics analysis of the robot structure. A graphical user interface is developed in order to visually verify and inspect robot link locations and the location of projected center of mass of developed robot. Theoretical and experimental results showed promising results on which we can build future biped robots.

Keywords: Humanoid robot; biped robot; mechanical design; kinematics

1 Introduction

Humanoid robots are hoped to take their rightful places in our daily lives [1]. With the increasingly aging developed countries' populations, robots that assist human activities in our environments such as in offices, homes and hospitals are expected. Especially, an emergence of humanoid robots is strongly expected because of anthropomorphism, friendly design, applicability of locomotion, behavior within the human living environments, and so on. To meet these demands, several humanoid robots have been developed Kaneko et al. [12]. Because of their anthropomorphic structure humanoid robots are ideal general-purpose assistant robots for performing typical everyday tasks in the human environment as stated by Buschmann et al. [7]. Humanoid robots could be classified into two main categories: human sized and small sized robots. Shirata et al. [24] classified humanoid robots as human sized robots have been developed mainly to study human-humanoid interaction and cooperation. On the other hand, it seems that the small sized robots are mainly aimed to entertainment applications. Some researchers focus on meeting the demand of game and

entertainment [21]. Yang et al. and Yoshikai et al. stated that [27 and 38] in order for humanoid robots to be able to assist humans at a very close distance, robots should allow contacts occurred at many places and deal with them without harming either parties. Azevedo et al. [5] argued that in nature, legs are adapted to cluttered environments allowing the machine to stride over obstacles and limiting the damages to the environment thanks to their small support surface. Since the early biped robots [1, 2, 13, 23 and 25] mass of the robots have been an important issue that needed to be addressed in many researches and it is stated strongly that it had to be minimised. Other than actuators, linking mechanisms have been constructed from lightest readily material available and it is usually some kind of aluminium alloys [5 and 9], which is 1060 series aluminium for our case. Kaneko et al. [12] used even lighter, aircraft grade aluminium alloys, and Park et al. [18] employed cast magnesium alloys for further lighten their robot. High rigidity and lightweight have been realized by adopting fiber reinforced plastic (FRP) and later carbon fiber rein-forced plastics (CFRP) as the major structural materials by Furuta T. and his co-researchers in their small scale humanoid robots.

As actuators for human size robots, most commonly used and practical drives are geared DC motors [1]. Some researchers use stepper motors but compared to DC ones, they develop quite small torques as used by Tar et al. [26]. Use of hydraulics and pneumatics are not practical either, due to their dependence on large air or hydraulic supply units, however, some examples of this type actuated robots exist [13]. McCibben type artificial muscles are being employed for their superior energy storage and impact damping abilities by Hosoda et al. [9]. However, these actuators have large hysteresis and are highly non-linear. Therefore, with these artificial muscles it is difficult to have precise position and speed control of joints, and not to mention problems about providing air source. For ease of communication with central control unit, digital servos are used by Tomoaki Yoshikai and his research group [28]. Placement of the geared motors defines the shape of mechanical parts. Hernández-Santos et al. and Medrano-Cerda et al. [8 and 15] placed electic motors horizontally for the sake of simplicity in their robot mechanisms. If motors were small enough, this orientation would pose no ill effect. However, longer motor sets (Motor + Gear head + encoder) stick out sideways and this placement makes the motor sets vulnerable to collision with external objects. Besides, it would not look natural for a humanoid robot. The employed motor sets are a bit longer than the smaller 20Watt motor sets perviously used by Akdas et al. [1 and 2]. Naturally, motor sets for sagittal plane joints had to be placed vertically at an angle. Arteaga et al. [4] used screw-nuts with satellite rollers combined with rod-crank systems, the nut with satellite rollers is inserted in a slider which is guided by usually four rollers that can move along a straight beam. This actuator configuration does not produce any significant perturbing parts. In this study, Maxon RE series motors with planetary gear heads and magnetic encoders are chosen.

Inertia of the legs of a biped robot affects the speed of locomotion. Vertical placement of the motor sets define the minimum length of the leg segments. It is proven by Buschmann et al. [7] that electric motors, located close to the hip joint axis, could reduce the thigh inertia up to 65% and the mass of the actuator itself by more than 10%, without reducing locomotion performance. For a human size biped robot, lengths of the links have to be comparable to humans', so that, it can successfully negotiate obstacles in human living environment. For this reason, vertical placement of the motor sets poses any significant problem. Legs and upper body had to be connected with a rigid structure that has very high stiffness coefficient as emphasized by Azevedo et al. [5]. In most of humanoid robots, strait aluminium plate is used to attach legs and the trunk of robots [5, 7, 9, 27 and 28]. In this study, an open "V" shape plate with upper and lower ridges on both sides are employed as main frame of the robot. Attaching lateral upper leg joints to angled sides of the "V" shape hip plate, enabled robot to be able to open its legs up to an angle of 120^{o}, which it is close to the most flexible human's. On board computing, necessary electronics and batteries significantly contribute the overall weight of the robot [19, 24 and 27]. In this work, the design process does not include on-board computing, batteries or power electronics. Other than small pre-processing electronics, all necessary data signal transmission carried out via screened cables. The pre-processed information from sensors that are on board the robot is sent to off-board electronics and then to a control computer. Off-board electronics include, some sensors, analogue voltage and power amplifiers, digital counter and multiplexer circuits. Other types of problems could arise when all necessary electronics, computers and batteries were to be placed on robot. Such as, the increased robot weight forces motor gear box ratios to be higher and joints need to be stronger. Finally, this leads to heavier and difficult to manage robots. The pros and cons of on-board and off board hardware of robots can be discussed further [10, 17 and 30]; however it is clear that eventually practical robots have to be free from all restrictions.

This paper focuses on designing human-size humanoid robot using relatively lightweight material and implementing rigid functional design features in a cost efficient way. The design promotes round and strait mechanical parts in order to cut down cost and production time. Since all the extremities are attached to the hip plate, it has to be highly rigid and at the same time low weight. The "finned V" plate is employed as a solution and initial test indicates that it satisfied all the expectations. The same plane joints of the robot leg are placed successively in order to simplify kinematic equations while this arrangement of joint order does not restrict the range of the motion. The joints' planes from ankle to hip of the leg are lateral ankle, sagittal ankle, sagittal knee, sagittal hip, lateral hip and top plane hip. The design also concurrently tried to keep inertia moments of legs at minimum. This is achieved by placing electric motor vertically and as close as possible to the hip plate. Embodied geared DC electric motors are opted to drive joints because of their relative ease of maintenance, lower costs and controllability. The design of assembly of mechanical parts with electric motors

includes ease of maintenance as they are shown in figures in following sections. Since, exploring mechanical design features and kinematic properties are also among the main objectives of the paper. One of the most prominent features of this robot design is its symmetric design in sagittal and in lateral planes. Lateral symmetry of robot's links enables robot potential movement sideways to left or right with equal motion range. Sagittal plane symmetry is the distinguishing feature of this robot from nearly all well-known bipedal humanoid robots. The sagittal ankle, knee and hip joint can rotate in both quadrants of the plane. The robot can locomote with straight knee and also while walking it can bend its knee at nominal angles (human like) or at traverse angles (chicken like). In this way, numerous locomotion strategies can be explored for all surface conditions of environment benefitting from unrestricted motion ranges. With this unrestricted motion range comes singularities (due to alignment of sagittal plane joints in vertical). This challenging problem makes the design more scientifically interesting and makes the further research to continue. Hence, a lot more care must be put in generation of locomotion trajectories for this robot in comparison to other biped robots [5, 12, 18 and 24], and this part forms the challenging next step of the research. To experiment for longer periods of time, the robot will be powered by off-board power supplies since the basic theories will be explored solely in the laboratory.

The rest of the paper is organized as follows. First, mechanical design issues are discussed in detail. Then, individual joint design criterions and their design are given in sub sections. The fourth section discusses motor selection and mathematical models. Finally, overall solved design issues and new revealed problems with the produced biped robot given in conclusion.

2 Design of Mechanical Parts

For walking forward and backward, sideways, climbing up and down the stairs and changing direction during locomotion, the robot has to have joints in all three orthogonal planes [1, 5, 6 and 24]. The robot has two lateral, three sagittal and one yaw joints in each leg. When designing joints as well as overall design of the robot, the following guidelines has been tried to be met.

a) Each joint should have single DoF for simplicity. This approach orthogonalizes and to eliminate offsets of joint axes of the robot enabling simpler dynamics of the robot.

b) Individual joint components have to be as straight as possible for ease of manufacturing using simple lathes and mills, also with least man power. In this way, cost of constructing a humanoid robot is minimized.

c) Joints have to be as rigid as possible avoid unwanted secondary motions.

d) Minimum number of components has to be used in joints for higher structural rigidity and maintenance of the robot hardware.

e) Lightest readily available material has to be used for economical and weight saving reasons.

f) Joint's range of motion have to be as large as possible and no mechanical constraints have to be employed in any joints including knees for providing wider work envelope.

g) Arrangement of joints should result in simpler analytic mathematical models. For this is in mind, starting left leg as a support leg or a base of open chain model, lateral ankle joint is chosen as the first joint of a tree structure. Then, three sagittal plane joints; ankle, knee and hip are constructed on top of lateral ankle. Same plane joints result in simpler mathematical models. Therefore, same plane joints should follow each other if possible. It is reiterated by Buschmann et al. [7] that design practice is an iterative and open-ended process of composition and simulation. After certain design milestones have been completed, updated inertia properties of the links and actuators are attained from the 3D-CAD models. These are used to calculate joint loads, workspaces and constraint forces using the dynamics simulation of the robot, which is the foundation for the dimensioning of actuators and mechanical components. In this way both simulation and CAD model are iteratively refined. In following subsections, detailed robot link and joint designs are given in detail.

2.1 Ankle Joints

Ankle joint is the base of the robot joint chain and Figure 1 shows rendered CAD design of lateral and sagittal ankle joints of the robot. The motor protection casing that is numbered as one in the picture is designed to surround motor + gearbox + magnetic encoder to take axial and radial loads on to itself. Radial ball bearings are placed on both sides of the load carrying and moving parts. Sagittal plane shaft is located just above the lateral joint casing. Conical matching gears (numbered as 4) (ratio is 1 to 1) transmit vertically placed motor's torque (numbered as 5 below) to sagittal plane horizontal shaft. Two vertical aluminum arms (numbered as 2) are designed to carry the whole load of the robot. A horizontal aluminum piece is attached to these vertical arms and motor gearbox, which forms a rigid structure. Also, small spacers are placed between shaft components in order to hold them tightly together. When the robot is in motion, the swing foot should clear ground. If for some reason contact occurs between the swing foot and the ground, the resultant torque at related joints of the robot can be sensed with the torque sensor. Shock and vibration absorption plates, made of rubber, are attached to the sole and toe of the foot.

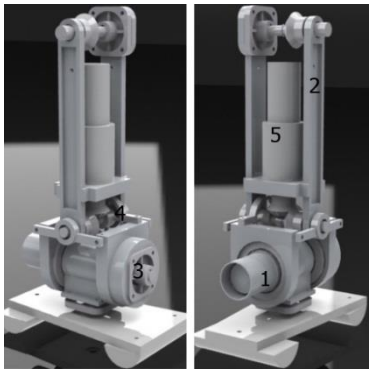

Figure 1
Lateral and sagittal ankle joints

2.2 Sagittal Knee and Hip Joints

The knee joint of the robot has no knee cap to restrict its motion. It can rotate in both quadrant in its plane of motion in order to simulate different types of locomotion. For instance, the robot can be used to realize human or chicken like locomotion types. Figure 2 shows ankle, knee and sagittal hip joints. Table 1 lists the range of motions that robot joints span. After assembly of the robot, the links of the robots are moved by hand and it is confirmed that the robot links can achieve the designed (in CAD environment) maximum range of motions as given in Table 1. The lack of knee cap creates singularity that can be problematic during locomotion. Effects of singularity can be minimized by careful design of joint trajectories. Also, good quality ultra-low backlash gear boxes could minimize the ill-effects of singularities. However, this was not the case for our biped robot which has up to 8 degrees of backlashes in some joints under nominal loadings. Therefore, joint trajectory generation becomes even more important than similar humanoid robots. A simple solution is that, during locomotion, sagittal plane leg joints always have to be loaded in one quadrant of the motion plane. Also, when particular joint needs to cross to the other side of the sagittal plane, it has to do so very smoothly and mono-directionally. Two 150 Watt DC motors power knee and hip links, which motors (numbered as 1 and 2 in Figure 2) are placed at 15 degrees of angles from vertical in opposite directions in order to fit them optimally in smallest bounding box.

Table 1
The range of motions of actual biped robot

Joint	Range	Joint	Range
Lat. Ankle	$\pm 45^0$	Lat. Trunk	$\pm 70^0$
Sag. Ankle	$\pm 40^0$	Sag. Trunk 1	$\pm 70^0$

Knee	$+100^0$,-90^0	Sag. Trunk 2	$\pm 70^0$
Sag. Hip	$\pm 50^0$	Sag. Shoulder	3 Full Rotation
Lat. Hip	$+120^0$, -50^0	Lat. Shoulder	$+130^0$, -15^0
Yaw Hip	3 Full Rotation	Yaw Shoulder	3 Full Rotation
Yaw Trunk	3 Full Rotation	Elbow	$\pm 45^0$

Zhao et al. [30] stated that the use of screw-nuts transmission mechanism that is adapted in some joints of lower limbs is to achieve compact and good dynamic performance. It is stated that for the knee and pitch motion of hip, screw-nuts transmitter to reduce the mechanical size and weight and for the yaw motion of ankle and hip. Also, the use of two bar linkage to provide variable transmission rate, which can provide more transmission rate at some conditions. However, these mechanisms usually are not back drivable and therefore there is no room for joint compliance and foot adaptability to any small objects that may lie on the ground. For these reasons, this type drive mechanism is not preferred in the robot. It is seen that some robots corporate coaxial joints with two degrees of freedom, timing belts and pulleys with bearings are installed to transmit mechanical power as in Yang et al. [27] work. This design feature is opted out in the robot design for reasons that belt and pulley mechanisms may not necessarily save space and reduce inertias. Also, secondary motions can be caused by uncontrollable play of belt mechanisms as a whole.

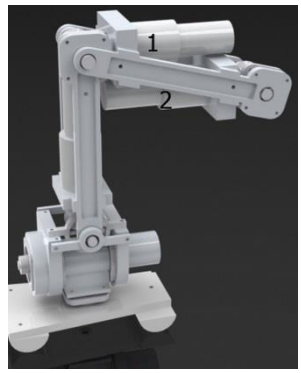

Figure 2
This figure shows bent knee joints

2.3 Midsection of the Robot

Figure 3 shows the mid-section of the robot (side support ridges are not shown). Lateral plane hip joints are placed underside of an open "V" shaped plate which its each arm is bent 30 degrees from horizontal. This joint orientation allows links to move about 60 degrees more in lateral than placing them on horizontal surfaces. Trunk yaw joint is also not restricted mechanically. However, internal cabling allows about three full rotations. All three joints are powered by 150 watt DC

motors which are attached to 156:1 ratio planetary gear heads and magnetic incremental encoders. In order to reduce loading effects, especially at sagittal plane joint motors, gravity compensations are employed in Saika-4 humanoid robot by Shirataet et al. [22]. It is important for humanoid robots to apply the gravity compensation to the legs to increase their performance. The gravity compensation mechanism is usually embedded in the legs. The mechanism use springs and compensates approximately a half of the required torque of the joints of the legs. The robot mechanism loading is directly affected by its joint trajectories during locomotion. The joint configuration in Figures 2 and 3 do not incorporate any gravity compensation mechanisms. Those design ideas are out of scope of this study, since design and manufacturing efficiencies are the major goals in our design approach.

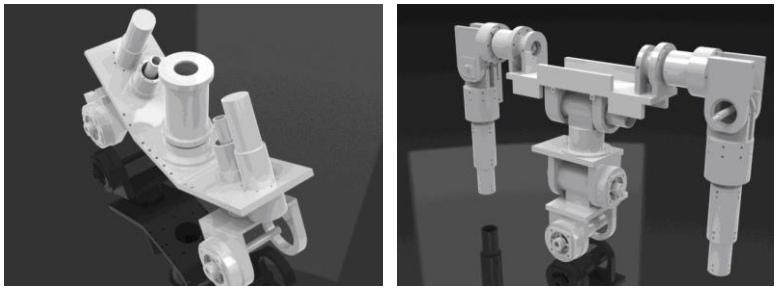

Figure 3
Lateral hip joints and trunk yaw joint and upper body of the biped robot

2.4 Upper Body of the Robot

Upper body of the robot consists of one lateral and two sagittal plane joints in the trunk and four joints in each arm. Direct axial and radial loading of motors are avoided by use of protection casing as in other joints. A 150 Watt motor is used in the lateral plane joints and 70 Watt motor are used in sagittal plane joints of trunk. 20 Watt motors are used in rest of the upper body. Figure 3 shows the structure of upper body of the robot.Geared motors directly drives joints minimizing the transmission losses. The robot has been designed to operate in known laboratory condition. Interaction with third persons are expected to be very limited. Also, attached safety cables prevents robot to fall down on to the floor. Parmiggiani et al and Wang et al. [19 and 28] stated that employment of torque limiter joint configurations is seen in some humanoid robot designs for above safety reasons for robots and humans

2.5 Assembled Robot

Shirata et al. [24] argued that the performance of the human sized humanoid robots is strictly limited by the performance of the electric motors, because the progress in the motors have not been remarkable compared with the progress in

the electronics. Therefore, the total mass of the robot and inertia properties of the links have been tried to be kept at minimum. Figure 4 shows the assembled biped robot without (on the left) and with (on the right) electrical connections. One of the thick umbilical cords carries sensor signals to PC and the other control carries signals back to the robot. As seen below, dedicated geared DC electric motors drive joints. Weak signals are carried via screened cables in order to minimize interference. The figure also shows the side mounted plastic gear pairs, which they are attached to joint shafts and potentiometers. Firstly, the positions of robot joints are read by these potentiometers, then with this information, the incremental encoder counter circuitries are initialized. The height of the robot is 155 cm and it weighs 55 kg. The aluminum frame makes up about 45% of the overall weight of the robot, the rest is geared electric motors and some electronic interface circuitry. Although it is produced from Aluminum, the weight is still a bit much. Therefore, the ease of handling of robot both during experiment and storage becomes an important issue as stated by Park et al. [18]. It is probable to harm on board electronics while handling. To reduce accidental damages to the robot, four cables are attached to the hip plate of the robot as shown in Figure 4. During experimentation, these cables are loosened to enable locomotion.

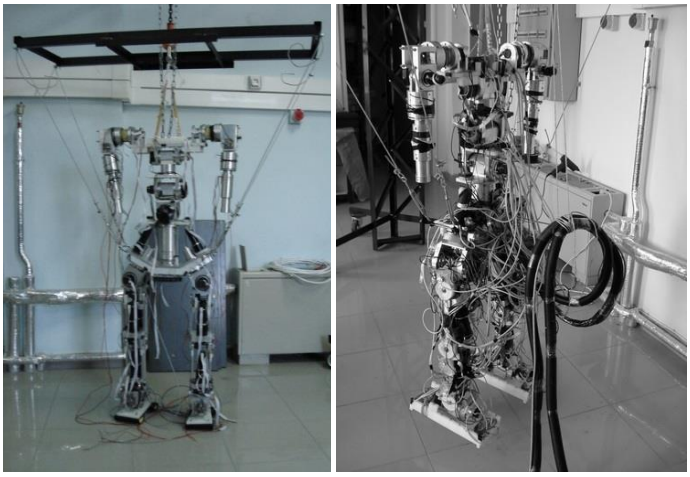

Figure 4

The figure on the left shows the completed mechanic assembly. The figure on the right shows fully assembled robot with umbilical cords to carry signals from and to the off-board electronics.

3 Motor Selection and Kinematic Modelling

For simpler driver circuitry and relative ease of control over other type of actuators, geared DC motors are chosen for the biped robot. From initial sketches, it is possible to estimate approximate weights and inertia properties of robot's

links by using CAD programs. With estimated parameters from kinematic equations and desired system performance specifications, suitable motor and gearbox combinations are chosen. Gearbox's gear ratio and rated torque values are two most important parameters that ultimately defines motion characteristics of the links. For this purpose, three types of motor and gearbox combinations are selected for the biped robots. Table 2 shows motor and gearbox combinations for each links. Some links require more driving torque, especially those of legs', than the others because of robot's geometry. Sagittal plane ankles, knees and hips are the most torque demanding links, therefore 150 Watt motor with gearbox of 30 Nm nominal torque which has 156:1 gear ratio is chosen. The intermittent torque value of the gearbox is 45 Nm. However, from experience, it is known that for short periods of operations, this maximum torque ratings can safely be exceeded.

Table 2

Table shows the links of the robot and their respected Maxon DC motor and gearbox combinations. All the gearboxes have same gearbox ratio of 156 to 1.

Link	Motor	Gearbox	Link	Motor	Gearbox
Lat. Ankle	70Watt	15Nm	Yaw Trunk	150Watt	30Nm
Sag. Ankle	150Watt	30Nm	Lat. Trunk	150Watt	30Nm
Knee	150Watt	30Nm	Sag1 Trunk	150Watt	30Nm
Sag. Hip	150Watt	30Nm	Sag2 Trunk	70Watt	15Nm
Lat. Hip	150Watt	30Nm	Rest of…	20Watt	6Nm
Yaw Hip	70Watt	15Nm			

The mathematical equations are in kinematic model forms and dynamic model forms. Kinematic models do not consider any speed and acceleration terms of the links. The only independent variable in this equation is relative joint orientations. In the case of dynamical mathematical models, relative joint positions, speeds and accelerations are considered as independent variables in dynamical mathematical models. Kinematic models are especially useful at initial joints toque estimation and joint trajectory generation for static locomotion.

3.1 Robot Kinematics

In static locomotion, resultant moments' force effects are relatively smaller than those of gravitational forces. As speed of locomotion increases, dynamical effects start to dominate effects of gravity. At higher speed of locomotion, the location of zero moment point is tracked rather than that of center of gravity [5, 18, 17 and 30]. As shown in Figure 5, three sagittal plane joints are placed successively. If lateral hip or ankle joints were placed, in between sagittal plane joints, the resulting kinematic equations would become up to 50% longer and more complex without virtually any difference in locomotion of trajectories of the robot between two joint placement sequences. Since the solutions of kinematic equations will be used in generation of joint trajectories, relatively simpler equations will be easier

to solve for inverse kinematics.Left leg is arbitrarily chosen as the basis of open chain kinematic structure of the robot.

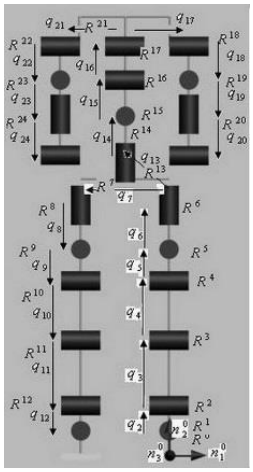

Figure 5

Figure shows inertial reference frame locations and the joints distances

Initially kinematics equations are used for estimation of joint torques of the robot for possible orientations of robot's posture. A simple way to calculate kinematic equations is presented below. It should also be considered to have an estimate of necessary relative joint orientations for some possible types of locomotion. This initial estimate helps us to shape the overall mechanical structure of the biped robot. For instance, if the robot is required to climb a 20 centimeter high step, then this requirement determines the constraints on biped robot's maximum joint angles and leg link's lengths. Hence, this gives size of torques and stress loading of joint linkages. Figure 5, the robot is in double support phase. Here, each cylinder represents single degrees of freedom (or direction of rotation) of the robot. Let R^k, *k=0,1,2…22* represent inertial reference frames. It is assumed that reference frames are located at respected joint rotation centers. n_j^k , *j=1, 2, 3* are orthogonal unit vectors at joint centers. $\mathbf{q}_l$, *l=0, 1, 2… 22* represents distances between the joints. Let m_k be lumped masses of links which are located by r_k positions vectors from the origin of respected inertial frames. θ_k are relative angles measured between successive links. g is the gravitational acceleration constant. The kinematics equations are used to obtain necessary joint angles for initial motor specifications and static locomotion joint trajectories. There is no unique way of choosing particular set of kinematics equations to solve for relative joint angles. Proper design of robot joint positions and orientation becomes the most important subject in later stages of the research where the joint trajectories needed to be generated. For this robotic study, minimum numbers of necessary (also sufficient) equations are derived for not over determination of joint trajectories

and for leaving room for modification of joint trajectories in their null spaces. For these reasons the following kinematic equation are chosen for the robot.

- The kinematics equations that give location of projection of center of gravity in three orthogonal directions.
- The kinematic equations that specify relative feet separations are also chosen, which they are also given in three orthogonal directions.

These equations can be written as following vector addition form. They are written starting from left foot as the base of the open kinematic chain to the other foot as given by Amirouche and Kane et al [3 and 11].

$$Sep = \sum_{i=2}^{12} q_i n^i \tag{1}$$

$$F_i = \left(\sum_{j=1}^{i-1} q_{j+1} n^j \right) + r_j n^i \tag{2}$$

$$G = \sum_{i=1}^{24} F_i m_i g \tag{3}$$

Equation 1 gives the distances between feet. Equations 2 and 3 gives the location of center of gravity forces. Additional joint constraint equations as well as limitations on joints angles can be added when solving these kinematic equations. For instance, a kinematics equation is written between support leg and one arm estimate distance between them. Equations 1 to 3 gives three dimensional nonlinear relations between robot links. The studies showed that planar nonlinear equations produce very close results. Figure 7 shows the amount of error in projected center of gravity locations between 2D and 3D equations. Using 2D kinematic equations instead of 3D kinematic equations produce less than 1 mm error in projected center of gravity. This small discrepancy is shown figure 7. Six kinematic equations can be written to define foot separations in 3 directions and location of projected center of mass in three directions. They are, foot separation in the direction of n_1 (side way), n_2 (height) and n_3 (forward or backward step), as well as the position of the COG in the direction of n_1, n_2 and n_3. A vector, from the left foot to right foot to find foot separations is the assumption here. Let $\boldsymbol{x}$ define the relative orientation vector as,

$$x = [\theta_1 \theta_2 \theta_3 \theta_4 \theta_5 \theta_6 \theta_7 \theta_8 \theta_9 \theta_{10}]^T \tag{4}$$

Let $\{q_1\}$ be the position vector from R_{i-1} to R_i, and $\boldsymbol{S_{ii-1}}$ be the transformation matrix from R_{i-1} to R_i. Then $\boldsymbol{S_{i0}}$ is

$$S_{i0} = \prod_{j=1}^{i} S_{j\ j-1} \tag{5}$$

Foot separation can be written as,

$$\{Sep\} = q_2 n_2^1 + q_3 n_2^2 + q_4 n_2^3 + q_5 n_2^4 + q_8 n_1^5 + q_9 n_2^8 + q_{10} n_2^9 \tag{6}$$

When this calculation is carried out,

$$Sep = Sep_{n1}n_1 + Sep_{n2}n_2 + Sep_{n3}n_3 \quad (7)$$

Sep_{n1} gives the sideways distance between the feet Sep_{n2} is the relative height of the feet, and Sep_{n3} is the step size. The 3D center of gravity equation can be written similarly to the planar equations. Let $\boldsymbol{m_i}$ ($i=1, 2...10$) mass of link i, and $\{\boldsymbol{r_i}\}$ be the vector from R_{i-1} to mass center of link i. Then, the location of center of gravity can be written as follows in a closed form,

$$COG^{3D} = \Big(m_1 r_1 n_2^1 + m_2(q_2 n_2^1 + r_2 n_2^2) + m_3(q_2 n_2^1 + q_3 n_2^2 + r_3 n_2^3) + m_4(q_2 n_2^1 + q_3 n_2^2 + q_4 n_2^3 + r_4 n_2^4) + m_5(q_2 n_2^1 + q_3 n_2^2 + q_4 n_2^3 + q_5 n_2^4 + r_5 n_2^5) + m_6(q_2 n_2^1 + q_3 n_2^2 + q_4 n_2^3 + q_5 n_2^4 + q_6(n_1^5 + n_2^5) + r_6 n_2^6) + m_7(q_2 n_2^1 + q_3 n_2^2 + q_4 n_2^3 + q_5 n_2^4 + q_6(n_1^5 + n_2^5) + q_7 n_2^6 + r_7 n_2^7) + m_8(q_2 n_2^1 + q_3 n_2^2 + q_4 n_2^3 + q_5 n_2^4 + q_8 n_1^5 + r_8 n_2^8) + m_9(q_2 n_2^1 + q_3 n_2^2 + q_4 n_2^3 + q_5 n_2^4 + q_8 n_1^5 + q_9 n_2^8 + r_9 n_2^9) + m_{10}(q_2 n_2^1 + q_3 n_2^2 + q_4 n_2^3 + q_5 n_2^4 + q_8 n_1^5 + q_9 n_2^8 + q_{10} n_2^9 + r_{10} n_2^{10})\Big) / m_{tot} \quad (8)$$

Here, m_{tot} is the total mass of the links. The calculation of equation 8 may look complex, however it is not more difficult than the derivation of planar center gravity equations especially with the help of a computer. Using transformation matrices $\boldsymbol{S_{i0}}$, equation 9 can be written in R. The intermediate calculations are skipped then. The final equation for center of gravity becomes

$$COG^{3D} = COG_{n1}n_1 + COG_{n2}n_2 + COG_{n3}n_3 \quad (9)$$

COG_{n1}, COG_{n2} and COG_{n3} are the three components of the center of gravity. The developed graphical user interface directly uses these equation to map them in a plot and output their value as shown in Figure 7. Below COG_{n1} is the component of the center of mass in the side direction. $s1 = sin(\theta_1)$, $c1 = cos(\theta_1)$, $s12 = sin(\theta_1 + \theta_2)$, $c12 = cos(\theta_1 + \theta_2)$ and the convention is the same for the remaining shorthand notations.

$T_{n1_1} = r_1 * g * m_1 * s_1$; $T_{n1_2} = -g * m_2 * (-q_2 * s_1 - r_2 * c_2 * s_1)$; $T_{n1_3} = -g * m_3 * (-q_2 * s_1 - q_3 * c_2 * s_1 - r_3 * c_{23} * s_1)$; $T_{n1_4} = -g * m_4 * (-q_2 * s_1 - q_3 * c_2 * s_1 - q_4 * c_{23} * s_1 - r_4 * c_{234} * s_1)$; $T_{n1_5} = g * m_5 * \Big(c_1 * (r_{5x} * c_5 + r_{5y} * s_5) + s_1 * \Big(q_2 + q_3 * c_2 + q_4 * c_{23} + c_{234} * (q_5 + r_{5y} * c_5 - r_{5x} * s_5)\Big)\Big)$; $T_{n1_6} = -g * m_6 * \Big(-s_1 * \Big(q_2 + q_3 * c_2 + q_4 * c_{23} + c_{234} * \big(q_5 + q_{6y} * c_5 + r_6 * c_{56} - q_{6x} * s_5\big)\Big) - c_1 * \big(q_{6x} * c_5 + q_{6y} * s_5 + r_6 * s_{56}\big)\Big)$; $T_{n1_7} == 1/2 * g * m_7 * \Big(\big(2 * c_1 * (q_{6x} * c_5 + q_{6y} * s_5 + (q_7 + r_7 * c_7) * s_{56}\big) + 2 * s_1 * \big(q_2 + q_3 * c_2 + q_4 * c_{23} + c_{234} * \big(q_5 + q_{6y} * c_5 + c_{56}(q_7 + r_7 * c_7) - q_{6x} * s_5\big) - r_7 * s_{234} * s_7\big)\Big)$; $T_{n1_8} = -g * m_8 * \Big(-s_1 * \big(q_2 + q_3 * c_2 + q_4 *$

$c_{23} + c_{234} * (q_5 - r_8 * c_{58} - q_8 * s_5)\big) + c_1 * (-q_8 * c_5 + r_8 * s_{58})\Big);$ $T_{n1_9} = -g * m_9 * (c_1 * (-q_8 * c_5 + (q_9 + r_9 * c_9) * s_{58}) - s_1 * (q_2 + q_3 * c_2 + q_4 * c_{23} - c_{234} * (q_5 + c_{58} * (q_9 + r_9 * c_9) + q_8 * s_5) + r_9 * s_{234} * s_9));$ $T_{n1\_10} = -g * m_{10} * \Big(-\Big(q_2 + q_3 * c_2 + q_4 * c_{23} + c_{234} * \big(q_5 - c_{58} * (q_9 + q_{10} * c_9 + r_{10} * c_{910})\big)\Big) * s_1 + c_1 * \Big(-q_8 * c_5 + (q_9 + q_{10} * c_9 + r_{10} * c_{910}) * s_{58}\Big) + s_1 * \big(q_8 * c_{234} * s_5 - s_{234} * (q_{10} * s_9 + r_{10} * s_{910})\big)\Big)\Big);$ (10)

$$COG_{n1} = \begin{pmatrix} T_{n1_1} + T_{n1_2} + T_{n1_3} + T_{n1_4} + T_{n1_5} + T_{n1_6} + T_{n1_7} \\ +T_{n1\_8} + T_{n1\_9} + T_{n1\_10} \end{pmatrix} / m_{tot} \quad (11)$$

COG_{n2} is the component of the center of mass in vertical direction is not currently being used in experiment, therefore its equations are not presented here. COG_{n3} is the component of the center of mass in the front direction.

$T_{n2_2} = r_2 * g * m_2 * c_1 * s_2;$ $T_{n2_3} = -g * m_3 * (-q_3 * c_1 * s_2 - r_3 * c_1 * s_{23});$ $T_{n2_4} = -g * m_4 * (-q_3 * c_1 * s_2 - q_4 * c_1 * s_{23} - r_4 * c_1 * s_{234});$ $T_{n2_5} = g * m_5 * c_1 * \Big(q_3 * s_2 + q_4 * s_{23} + s_{234} * \big(q_5 + r_{5y} * c_5 - r_{5x} * s_5\big)\Big);$ $T_{n2_6} = g * m_6 * c_1 * \Big(q_3 * s_2 + q_4 * s_{23} + s_{234} * \big(q_5 + q_{6y} * c_5 + r_6 * c_{56} - q_{6x} * s_5\big)\Big);$

$T_{n2_7} = g * m_7 * c_1 * \big(q_3 * s_2 + q_4 * s_{23} + s_{234} * \big(q_5 + q_{6y} * c_5 + c_{56} * (q_7 + r_7 * c_7) - q_{6x} * s_5\big) + r_7 * c_{234} * s_7\big);$ $T_{n2_8} = g * m_8 * c_1 * \big(q_3 * s_2 + q_4 * s_{23} + s_{234} * (q_5 - r_8 * c_{58} - q_8 * s_5)\big);$ $T_{n2_9} = g * m_9 * c_1 * (q_3 * s_2 + q_4 * s_{23} - s_{234} * (-q_5 + c_{58} * (q_9 + r_9 * c_9) + q_8 * s_5) - r_9 * c_{234} * s_9);$ $T_{n2_{10}} = -g * m_{10} * c_1 * (-q_3 * s_2 - q_4 * s_{23} - q_5 * s_{234} + q_9 * c_{58} ** s_{234} + q_{10} * c_{58} * c_9 * s_{234} + r_{10} * c_{58} * c_{910} * s_{234} + q_8 * s_{234} * s_5 + q_{10} * c_{234} * {c_{58}}^2 * s_9 + q_{10} * s_{234} * c_8 * s_5 * s_{58} * s_9 + q_{10} * c_{234} * c_5 * s_8 * s_{58} * s_9 + r_{10} * c_{234} * s_{910});$ (12)

$$COG_{n3} = \begin{pmatrix} T_{n2_2} + T_{n2_3} + T_{n2_4} + T_{n2_5} + T_{n2_6} + T_{n2_7} + T_{n2_8} \\ +T_{n2\_9} + T_{n2\_10} \end{pmatrix} / m_{tot} \quad (13)$$

It is important to know relative foot separation values in three dimension too. Since the robot has been designed to walk statically, one foot is always is assumed to be firmly on ground. The relative position of the swing foot with respect to support foot has to be known at all times. These equations are quite trivial to obtain. In order to obtain the relative foot separation values, vector must be added starting from support foot and ending up at swing foot as in equation 6 and 7. So 3D non-linear relative foot separation equations becomes,

$C_{n1\_1} = -q_8 * c_1 * c_5 - q_2 * s_1 - q_3 * c_2 * s_1 - q_4 * c_{23} * s_1 - q_5 * c_{234} * s_1 + q_5 * c_{234} * c_{58} * s_1 + q_4 * c_{234} * c_{58} * c_9 * s_1 + q_3 * c_{10} * c_{234} * c_{58} * c_9 * s_1;$

$C_{n1\_2} = -q_3 * c_9 * s_1 * s_{10} * s_{234} + q_8 * c_{234} * s_1 * s_5 + q_5 * c_1 * s_{58} + q_4 * c_1 * c_9 * s_{58} + q_3 * c_1 * c_{10} * c_9 * s_{58} - q_3 - c_{234} * c_{58} * s_1 * s_{10} * s_9 - q_4 * s_1 * s_{234} * s_9;$

$$C_{n1\_3} = -q_3 * c_{10} * s_1 * s_{234} * s_9 - q_3 * c_1 * s_{10} * c_{58} * s_9; \quad (14)$$

$$C_{n1} = C_{n1\_1} + C_{n1\_2} + C_{n1\_3} \quad (15)$$

$$C_{n2\_1} = q_2 * c_1 + q_3 * c_1 * c_2 + q_4 * c_1 * c_{23} + q_5 * c_1 * c_{234} - q_5 * c_1 * c_{234} * c_{58} - q_4 * c_1 * c_{234} * c_{58} * c_9 - q_3 * c_1 * c_{10} * c_{234} * c_{58} * c_9 - q_8 * c_5 * s_1;$$

$$C_{n2\_2} = q_3 * c_1 * c_9 * s_{10} * s_{234} - q_8 * c_1 * c_{234} * s_5 + q_5 * s_1 * s_{58} + q_4 * c_9 * s_1 * s_{58} + q_3 * c_{10} * c_9 * s_1 * s_{58} + q_3 * c_1 * c_{234} * c_{58} * s_{10} * s_9 + q_4 * c_1 * s_{234} * s_9;$$

$$C_{n2\_3} = q_3 * c_1 * c_{10} * s_{234} * s_9 - q_3 * s_1 * s_{10} * s_{58} * s_9; \quad (16)$$

$$C_{n2} = C_{n2\_1} + C_{n2\_2} + C_{n2\_3} \quad (17)$$

$$C_{n3\_1} = -q_3 * c_{234} * c_9 * s_{10} + q_3 * s_2 + q_4 * s_{23} + q_5 * s_{234} - q_5 * c_{58} * s_{234} - q_4 * c_{58} * c_9 * s_{234} - q_3 * c_{10} * c_{58} * c_9 * s_{234} - q_8 * s_{234} * s_5;$$

$$C_{n3\_2} = -q_4 * c_{234} * s_9 - q_3 * c_{10} * c_{234} * s_9 + q_3 * c_{58} * s_{10} * s_{234} * s_9; \quad (18)$$

$$C_{n3} = C_{n3\_1} + C_{n3\_2} \quad (19)$$

Where, C_{n1}, C_{n2} and C_{n3} are foot separation values in three orthogonal directions. The directions of unit vectors n_1, n_2 and n_3 is shown in Figure 5. During experimentation, robot's control systems checks the location of COG_{n1}, COG_{n2}, COG_{n3}, C_{n1}, C_{n2} and C_{n3} a hundred times a second and compares the results to predetermined trajectories for these. Dynamical equations are to be used to design stabilizing controller for the robot. These dynamical equations are to be used in simulations, in their full nonlinear forms, to test control system under given joint reference angles, as well. Since, this paper does not cover those control system design procedures and their simulations. However, they are planned to be presented in the following publications, once they are completed and analyzed thoroughly.

4 Simulation Results and Discussion

The humanoid robot research at Balikesir University promotes simple yet functional mechanical part designs that lead to cost efficient part manufacturing. Figure 4 shows mechanical assembly of the humanoid robot. All parts fitted perfectly along with geared DC motors, whose power ratings were given in Table 2. Considering the total production cost around 15000 Euros and two weeks of manufacturing time for the mechanical parts proves the effectiveness of the design. Magnetic encoders and potentiometers are used to measure relative angle between the robot links. After the assembly of the robot, the links are moved by hand and it is confirmed that the robot links can achieve the designed maximum range of motions as given in Table 1. Initial experiments showed the success of the design where the orthogonal joint structure is quite rigid and do not allow any

significant unwanted secondary motions. The "V" shaped hip base plate is well suited to attach upper and lower parts of the robot. However, the normal distance between the legs is a bit long. As a result, in order to shift the center of gravity in the lateral plane, the upper part of the robot has to move almost 60 degrees to sideways. Although this does not pose much of a problem, shortening the normal distance between the legs in the lateral plane would reduce the travel time of the robot's upper body. For that sense, it would be better if the hip width were to be minimised in the next generation of robots. Stabilizing control system for the whole of the robot has not been tested yet. However, even with simple, single input single output PD-type controller, triangular shape reference tracking performed on sagittal plane left hip joint. Single joint reference tracking test is performed to show the design goal is met and mechanics of the system enabling even the simplest control technique to perform satisfactorily. In Figure 6, red colour line indicates desired joint reference and blue colour line shows actual joint position. The tracking error is less than 0.2 degrees that is within the backlash zone of the used gearboxes. Although more robust techniques are available as suggested by Precup et al. [20] to cater for parameter variation, these advanced control techniques are not yet a necessity at this initial testing stage of the humanoid robot.

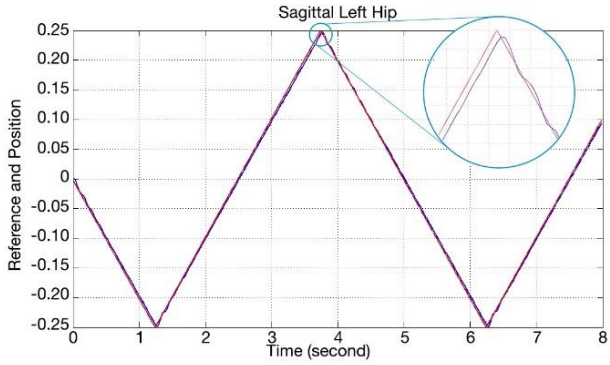

Figure 6

Sagittal plane left hip joint, triangular reference tracking using simple SISO PD controller

Advantage of the adopted kinematic scheme is proven in Figure 7. The difference between 2D and 3D equations in locating center of gravity is less than 1mm at a 30 cm step size. Equation 8 gives the closed form of 3D central gravity location equation. Its open form is about 5 pages long and it takes quite a long time to solve even when the numerical solution is not stuck at one of the local minima. Therefore, 2D equations 11, 13, 15, 17 and 19 produce much faster and easier solutions to the problem of joint trajectory location. Figure 7 shows the graphical user interface (GUI) that utilizes given kinematic equations. GUI is also in early stages of its development. Once a set of joint angle values is given, it uses 3D equations to calculate joint positions and location of COG, and draws them using straight lines. When the play button is pressed, the counter inside the program

increases and re-evaluates kinematic equations and refreshes the plot area. In future, real-time data from robot joints will be superimposed to reference simulation data for comparison. This GUI gives visual feedback to evaluate generated reference points. The mechanical design methodology has proved itself as a cost effective and functional humanoid robot. Up to this point, the control system has been tested on a single joint in order to evaluate motion tracking capabilities of the system. Rigid mechanical system helped the control system perform very satisfactorily. From now on the research focuses on obtaining whole body dynamical equations on which the control system is planned to be based.

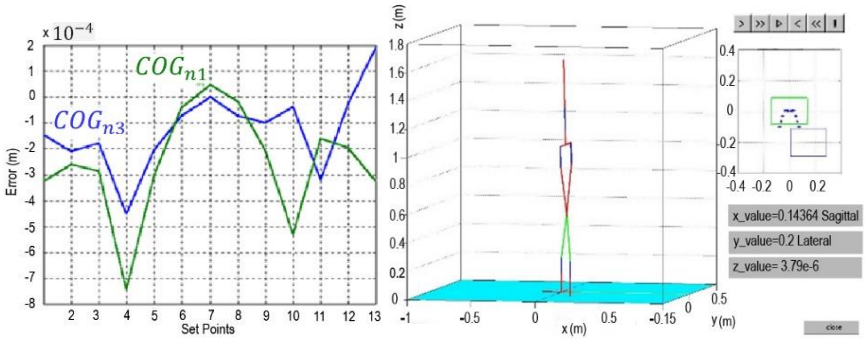

Figure 7

Error in the trajectory of center of gravity (COG) (left figure) when 3D non-linear kinematic equations are evaluated with the solutions of 2D linearized kinematic equations. Here, n3 is the front and n1 is the side direction. The graphical User Interface (right figure) of the robot displays kinematical properties of the robot such as relative foot separation and location of centre of gravity.

Conclusions

This paper aims to introduce the mechanical design process of the experimental human-size biped robot at Balikesir University. Adopted mechanical part design methodology has proven itself very effective in terms of production time and cost. Straight and round shaped mechanical parts formed single degree of freedom joints and "V" shaped hip plate created rigid structure as a base for robot extremities. The robot is relatively lightweight considering its size. By placing sagittal plane leg motor sets in vertical angles helped lower the inertias. The governing differential equations of humanoid robots are quite complex. The developed humanoid "BUrobot" has successive sagittal plane joints in its legs. This arrangement of joints has resulted in simpler and shorter kinematic equations as given in section 3. The robot joints motion symmetry in both quadrants from vertical is preserved. This unique mechanical property of robot joints will enable unrestricted trajectory generations by permitting the knees to bend human-like or chicken-like, whereas this locomotion property may be useful in rough or constricted terrains. For successful locomotion, the relative position of feet and location of COG must be known. Nonlinear 2D and 3D kinematic equation are obtained and they are compared with each other for accuracy. It is proven that for

small step sizes both equations produce very close results. In order visually inspect the joint angles' effects in terms of foot separation and projected center of gravity, a simple GUI is developed. In future, the program will be further developed to enable real experimental data and simulation data to be superimposed for comparison and evaluations purposes. Mechanical properties of robot such as light weight, low inertia and joint rigidity is tested in single joint for closed loop reference tracking. Initial test proves the effectiveness of the design even with simple PD controller. The research will continue to develop full nonlinear differential equations and design of stabilizing control systems.

Acknowledgement

The research was sponsored by "The Scientific and Technological Research Council of Turkey" (TUBITAK) for sponsoring this biped robot research, and Balikesir University, Academic Research Projects Council.

References

[1] Akdas D. and Medrano-Cerda G. A.: Design of a Stabilizing Controller for a 10-degree of Freedom Bipedal Robot Using Linear Quadratic Regulator Theory, Proceedings of the Institution of Mechanical Engineers Part C, Vol. 215, No C1, pp. 27-43

[2] Akdas D. and Medrano-Cerda G. A.: Single Support Static Balancing of a 12 DOF Biped Robot, 2nd International conference on Climbing and Walking Robots, CLAWAR99, pp: 143-147, Portsmouth 13-15 Sept. 1999

[3] Amirouche F. M. L.: Computational Methods in Multibody Dynamics, Prentice-Hall, New Jersey

[4] Arteaga M. A.: Castillo-Sáncheza A. and Parra-Vegab, V., Cartesian Control of Robots without Dynamic Model and Observer Design, Elsevier Automatica Vol. 42, 473-480, 2006

[5] Azevedo C., Andreff N. and Arias S.: BIPedal Walking: from Gait Design to Experimental Analysis, Elsevier Mechatronics Vol. 14, 639-665, 2004

[6] Bruneau O.: An Approach to the Design of Walking Humanoid Robots with Different Leg Mechanisms or Flexiable Feet and Using Dynamics Gaits, 10 bvd Lahitolle 18020 Bourges Cedex, France, 1457-1482, 24 May 2006

[7] Buschmann T., Lohmeier S. and Ulbrich, H.: Humanoid Robot Lola: Design and WAlking Control, Journal of Physiology Paris Vol. 103, 141-148, 2009

[8] Hernández-Santos C, Rodriguez-Leal1 E, Soto R and Gordillo J. L: Kinematics and Dynamics of a New 16 DOF Humanoid Biped Robot with Active Toe Joint, International Journal of Advanced Robotic Systems, DOI: 10.5772/52452, 2012

[9] Hosoda K., Takuma T., Nakamoto A. and Hayashi, S.: Biped Robot Design Powered by Antagonistic Pneumatic Actuators for Multi-Modal Locamotion, Elsevier Robotics and Autonomous Systems Vol. 56, 46-53, 2008

[10] Hosoda K., Takuma T. and Nakamoto A.: Design and Control of 2D Biped that can Walk and Run with Pneumatic Artifical Muscles, IEEE Humanoids 1-4244-0200, 284-289, 2006

[11] Kane, T. R. and Levinson D. A.: Dynamics Theory and Applications, McGraw-Hill, ISBN 0-07-037846-0

[12] Kaneko K., Kanehiro F., Kajita S., Hirukawa H., Kawasaki T., Hirata M., Akachi K. and Isozumi T.: Humanoid Robot HRP-2, Proceedings of the 2004 IEEE Int. Conference on Robotics & Automation New Orleans - LA, 1083-1090, April 2004

[13] Kato I and Tsuiki H.: Hydraulically Powered Biped Walking Machine with a High Carrying Capacity, Proceedings of the 4th International Symposium on External Control of Human Extremities, pp. 410-421, 1972

[14] Löffler K., Gienger M. and Pfeiffer F.: Sensor and Control Design of a Dynamically Stable Biped Robot, Proceedings of the 2003 IEEE Int. Conference on Robotics & Automation Taipei, Taiwan, 484-490, September 14-19 2003

[15] Medrano-Cerda G. A. and Eldukhri E. E.: Biped Robot Locomotion in the Sagittal Plane, Transactions Instrument Measurement and Control, 1997, Vol. 19, No. 1, pp. 38-49

[16] Medrano-Cerda G. A. and Akdas D.: Stabilization of a 12 Degree of Freedom Biped Robot, Proceedings of the 15th IFAC World Congress, 2002, Volume 15, Part 1

[17] Ouezdou F.B., Mohamed B., Scesa V. and Sellaouti R.: Design and Experiments of a Torso Mechanism for the ROBIAN Biped Robot, Robotica Vol. 24, 337–347, 2006

[18] Park W, Kim J. Y, Lee J and Oh, J. H: Mechanical Design of Humanoid Robot Platform KHR-3, Proceedings of 2005 5th IEEE-RAS International Conference on Humanoid Robots, 2005

[19] Parmiggiani A., Maggali M., Natale L., Nori F., Schmitz A., Tsagarakis N., Victor J. S., Becchi F., Sandini G. and Metta G.: The Design of the Icub Humanoid Robot, International Journal of Humanoid Robotics WSPC-Instruction File ijhrPaper, 1-23, 2011

[20] Precup R. E. and Preitl S.: PI and PID Controllers Tuning for Integral-Type Servo Systems to Ensure Robust Stability and Controller Robustness, Electrical Engineering, Vol. 88, No. 2, pp. 149-156, 2006

[21] Qiubo P., Qishu H., Bingrong and Songhao P.: Design and Implementation of Humanoid Robot HIT-2, Proceedings of the IEEE International Conference on Robotics and Biomimetics Bangkok, Thailand, February 21 - 26, 967-970, 2009

[22] Sakagami Y., Watanabe R., Aoyama C., Matsunaga S., Higaki N. and Fujimura K.: The Intelligent ASIMO: System Overview and Integraion, Proceedings of the 2004 IEEE/RSJ Int. Conference on Intelligent Robots and Systems EPFL, Lausanne – Switzerland, 2478-2483, October 2004

[23] Santos V., Moreira R. and Silva F.: Mechatronic Design of a New Humanoid Robot with Hybrid Parallel Actuation, International Journal of Advanced Robotic Systems, DOI: 10.5772/51535, Vol. 9, 119:2012

[24] Shirata S., Konno A. and Uchiyama M.: Design and Development of a Light-Weight Biped Humanoid Robot Saika-4, Proceedings of 2004 IEEE|RSJ International Conference on Intelligent Robots and Systems, Sendai-Japan, 148-153, September 28 October 2, 2004

[25] Takanishi A, Ogura Y and Itoh K.: Some Issues in Humanoid Robot Design, Robotics Research, Springer Tracts in Advanced Robotics, DOI:10.1007/978-3-540-48113-3_32, Volume 28, pp 357-372, 2007

[26] Tar A. Veres J., Cserey G.: Design and Realization of a Biped Robot Using Stepper Motor Driven Joints, IEEE 3rd International Conference on Mechatronics, 493-498, 2006

[27] Yang H. S., Seo Y., Chae Y., Jeong W., Kang W. and Lee J.: Design and Development of Biped Humanoid Robot, AMI2, for Social Interaction with Humans, 1-4244-0200-X/06/$20.00 IEEE Humanoids, 352-357, 2006

[28] Yoshikai T., Hayashi T., Kadowaki M., Goto A. T. and Inaba M.: Design and Development of a Humanoid with Soft 3D-Deformable Sensor Flesh and Automatic Recoverable Mechanical Overload Protection Mechanism, The 2009 IEEE/RSJ International Conference on Intelligent Robots and Systems, St. Louis USA, 4977-4983, October 11-15 2009

[29] Wang T., Chevallereau C. and Rengifo C. F.: Walking and Streering Control for a 3D Biped Robot Considering Ground Contact and Stability, Robotics and Autonomous Systems - Elsevier Vol. 60, 962–977, 2012

[30] Zhao M., Liu L., Wang J., Chen K., Zhao J. and Xu K.: Control System Design of THBIP-I Humanoid Robot, Proceedings of the 2002 IEEE International Conference on Robotics 8 Automation Washington- DC, 2253-2258, May 2002